










# FLOWERING REPRESSOR AAA<sup>+</sup> ATPase 1 is a novel regulator of perennial flowering in *Arabis alpina*

Natanael Viñegra de la Torre<sup>1,2,3</sup> , Alice Vayssières<sup>1,2,3,\*</sup> , Evelyn Obeng-Hinne<sup>1,2,3,\*</sup>, Ulla Neumann<sup>2</sup> ,  
Yanhao Zhou<sup>1,2,3</sup> , Ana Lázaro<sup>1,2,3</sup>, Adrian Roggen<sup>1,2</sup>, Hequan Sun<sup>2</sup> , Sara C. Stolze<sup>2</sup> ,  
Hirofumi Nakagami<sup>2</sup> , Korbinian Schneeberger<sup>2</sup> , Ton Timmers<sup>2</sup> and Maria C. Albani<sup>1,2,3,4</sup> 

<sup>1</sup>Institute for Plant Sciences, University of Cologne, Zùlpicher Str. 47b, 50674 Cologne, Germany; <sup>2</sup>Max Planck Institute for Plant Breeding Research, Carl-von-Linné Weg 10, 50829

Cologne, Germany; <sup>3</sup>Cluster of Excellence on Plant Sciences “From Complex Traits towards Synthetic Modules”, 40225 Düsseldorf, Germany; <sup>4</sup>Present address: Rijk Zwaan, Burgemeester Crezélaad 40, PO Box 40, 2678 ZG De IJser, the Netherlands

## Summary

Author for correspondence:  
Maria C. Albani  
Email: [albani@mpipz.mpg.de](mailto:albani@mpipz.mpg.de)

Received: 10 February 2022  
Accepted: 4 July 2022

New Phytologist (2022) 236: 729–744  
doi: 10.1111/nph.18374

**Key words:** AAA<sup>+</sup> ATPase, *Arabis alpina*,  
flowering, FRAT1, PEP1, perennial,  
peroxisomes, vernalization.

- *Arabis alpina* is a polycarpic perennial, in which PERPETUAL FLOWERING1 (PEP1) regulates flowering and perennial traits in a vernalization-dependent manner. Mutagenesis screens of the *pep1* mutant established the role of other flowering time regulators in PEP1-parallel pathways.
- Here we characterized three allelic *enhancers of pep1* (*eop002*, *085* and *091*) which flower early. We mapped the causal mutations and complemented mutants with the identified gene. Using quantitative reverse transcriptase PCR and reporter lines, we determined the protein spatiotemporal expression patterns and localization within the cell. We also characterized its role in *Arabidopsis thaliana* using CRISPR and in *A. alpina* by introgressing mutant alleles into a wild-type background.
- These mutants carried lesions in an AAA<sup>+</sup> ATPase of unknown function, *FLOWERING REPRESSOR AAA<sup>+</sup> ATPase 1* (*AaFRAT1*). *AaFRAT1* was detected in the vasculature of young leaf primordia and the rib zone of flowering shoot apical meristems. At the subcellular level, *AaFRAT1* was localized at the interphase between the endoplasmic reticulum and peroxisomes. Introgression lines carrying *Aafrat1* alleles required less vernalization to flower and reduced number of vegetative axillary branches. By contrast, *A. thaliana* CRISPR lines showed weak flowering phenotypes.
- *AaFRAT1* contributes to flowering time regulation and the perennial growth habit of *A. alpina*.

## Introduction

During the course of evolution, flowering plants have evolved different life history strategies, mostly related to their capacity to reproduce during their life cycle. From this perspective, most plants can be classified as monocarpic or polycarpic, depending on how many times they are able to undergo a reproductive phase during their lifetime. Annual plants are usually monocarpic, as they are able to complete their life cycle within a year, dying shortly after they have flowered and set seeds. Conversely, perennial plants are generally polycarpic, meaning that they will experience several reproductive phases during their lifetime, while they persist in the environment (Li *et al.*, 2021). To achieve this, perennial plants usually show asynchronous development of meristems, which allows them to concentrate their reproductive effort only in certain parts, whereas the rest of the plant remains vegetative (Amasino, 2009). The model plant *Arabis alpina*

presents a polycarpic perennial life habit. In addition, some accessions (e.g. Pajares) show a strong vernalization requirement, hence remaining vegetative until they experience prolonged periods of cold (Wang *et al.*, 2009). The use of comparative studies between *A. alpina* and its annual relative *Arabidopsis thaliana* has allowed the identification of floral regulators with common but also distinct functions between these species, which can be indicative of differential adaptation regarding life history strategies (Albani & Coupland, 2010).

Recent studies have identified key genes involved in the perennial flowering of *A. alpina* (Wang *et al.*, 2009, 2011; Bergonzi *et al.*, 2013; Hyun *et al.*, 2019; Lázaro *et al.*, 2019). One such core regulator of flowering in response to vernalization is *PERPETUAL FLOWERING1* (*PEP1*), which is a MADS domain transcription factor and the orthologue of *A. thaliana* *FLOWERING LOCUS C* (*FLC*) (Wang *et al.*, 2009). Similar to *FLC* in *A. thaliana*, vernalization results in the repression of *PEP1* expression, which allows some meristems in the plant to

\*These authors contributed equally to this work.

transition into the reproductive phase and flower (Sheldon *et al.*, 2000; Lázaro *et al.*, 2018). After vernalization, *PEP1* is upregulated, ensuring the maintenance of vegetative development in some axillary meristems and contributing to the overall perennial life history in *A. alpina*. Accordingly, *pep1* mutant alleles show reduced life span in field experiments (Hughes *et al.*, 2019).

Other examples of floral regulators with additional functions in *A. alpina* include factors that regulate the age-dependent response to vernalization, for example the *A. alpina* *TERMINAL FLOWER 1* (*AaTFL1*), the *APETALA2* transcription factors *PEP2* and *TARGET OF EAT2* (*AaTOE2*), and the *A. alpina* *SQUAMOSA PROMOTER-BINDING PROTEIN-LIKE 15* (*AaSPL15*). These genes were shown to affect the age at which plants become competent to respond to flowering-inducing signals, the duration of vernalization they required for flowering and the maintenance of vegetative growth in axillary meristems (Wang *et al.*, 2011; Hyun *et al.*, 2019; Lázaro *et al.*, 2019; Zhou *et al.*, 2021). Despite its prominent role in vernalization, *PEP1* is not the only regulator in this pathway as *pep1* mutants still respond to prolonged cold treatments (Lázaro *et al.*, 2018). In an effort to identify other regulators of flowering apart from *PEP1*, the *pep1-1* mutant was used as background for an EMS (ethyl methanesulphonate) mutagenesis screen for *enhancers of pep1* (eop; Zhou *et al.*, 2021).

In this study we characterized three members of the *eop* mutant population, namely *eop002*, *eop085* and *eop091*, which showed an extremely early flowering phenotype in long day (LD) conditions compared to *pep1-1*. These three mutants are allelic and all carry mutations in the coding sequence of a member of the AAA<sup>+</sup> superfamily of ATPases, which we named *FLOWERING REPRESSOR AAA<sup>+</sup>-ATPase 1* (*AaFRAT1*). By resequencing *AaFRAT1* in our *eop* mutant collection, we detected 14 *eop* mutants carrying lesions in *AaFRAT1*, suggesting that it may play an instrumental role in the development of *A. alpina*. Furthermore, *A. alpina* lines carrying the *Aafrat1* mutant alleles in the Pajares wild-type background, which requires vernalization to flower, showed compromised perennial traits and required shorter durations of vernalization to flower. At the shoot apical meristem, we detected *AaFRAT1* mostly in the vasculature of young leaf primordia and very faintly at the rib zone. At the subcellular level, *AaFRAT1* was localized at the interphase between endoplasmic reticulum (ER) tubules and peroxisomes (in seedling roots). In *A. thaliana*, the *AaFRAT1* orthologue belongs to a cluster of four tandemly duplicated genes. *Atfrat1* CRISPR mutants in *A. thaliana* showed very mild flowering time phenotypes, suggesting that the role of *AtFRAT1* on flowering is not as prominent as that of *AaFRAT1* in *A. alpina*. Our study is the first to demonstrate the involvement of a member of the AAA<sup>+</sup> family of ATPases in flowering, which will open new pathways for future research.

## Materials and Methods

### Plant materials, growth conditions and phenotypic analyses

Experiments with *A. alpina* L. were performed with the accession Pajares or with mutants obtained in this background. The *pep1-1*

mutant was previously obtained from a mutagenesis screen of the *A. alpina* accession Pajares (Wang *et al.*, 2009). The *enhancers of pep1* mutants (*eop*) were obtained from an enhancer screen of *pep1-1* (Zhou *et al.*, 2021). The *eop002*, *eop085* and *eop091* mutant phenotypes were subsequently confirmed in the M3 generation and are first described in this study. Experiments in *A. thaliana* L. were performed in the accession Col-0.

Flowering time experiments in both species were performed either in a long day (LD; 16 h : 8 h, light : dark) or a short day (SD; 8 h : 16 h, light : dark) glasshouse at 18–21°C or after a vernalization treatment at 4°C and SD conditions (in the case of *A. alpina*). Vernalization experiments were performed by growing plants first in an LD glasshouse for 8 wk, exposing them to cold treatment (4°C and SD) for 8–18 wk and returning them to an LD glasshouse.

For hypocotyl elongation experiments, seeds were surface-sterilized with chlorine gas for 3 h and sowed in plates containing 1% agar ½ Murashige & Skoog medium (w/v) under sterile conditions. After sowing, plates were incubated for 3 d at 4°C in the dark for seed stratification. Subsequently, seed plates were exposed to 6 h (Arabidopsis) or 10 h (Arabis) of light to trigger germination. After this period, plates were covered and left in the dark for 5 d in an LD growth cabinet (16 h : 8 h, light : dark, at constant 21°C). Seedlings were then stretched onto fresh plates and scanned. All measurements were performed using IMAGEJ (Schneider *et al.*, 2012).

### Mapping by sequencing and fine mapping

For mapping-by-sequencing of the mutants, we created three BC1F2 mapping populations by backcrossing *eop002*, *eop085* or *eop091* with *pep1-1*, respectively. These segregating populations (768 individuals for *eop002*BC1F2, 980 for *eop085*BC1F2 and 768 for *eop091*BC1F2) were grown in an LD glasshouse and the earliest flowering BC1F2 plants from each population were selected for further analysis (96 *eop002*BC1F2, 96 *eop085*BC1F2 and 134 *eop091*BC1F2). Flower buds from selected plants were pooled from each population and their DNA was isolated using a DNeasy<sup>®</sup> Plant Minikit (Qiagen), and subsequently sequenced with an Illumina HiSeq2000 (Illumina) at the Max Planck Genome Centre Cologne (Germany). We obtained 138.04 million reads for the *eop002*BC1F2 pool, 30.15 million for the *eop085*BC1F2 pool and 161.84 million for the *eop091*BC1F2 pool. From these reads, 94.86% of the *eop002*BC1F2 pool, 96.12% of the *eop085*BC1F2 pool and 93.44% of *eop091*BC1F2 were aligned to the *A. alpina* V5 reference genome using BOWTIE 2 (Langmead & Salzberg, 2012; Jiao *et al.*, 2017), resulting in an average coverage of 89.2 for *eop002*BC1F2, 20.83 for *eop085*BC1F2 and 102.9 for *eop091*BC1F2 for the respective resequenced genome. For reference we used the *pep1-1* genome, as described in Zhou *et al.* (2021). SAMTOOLS and BCFTOOLS were applied to identify single nucleotide polymorphisms (SNPs) between the BC1F2 pools and the *A. alpina* reference genome (Li *et al.*, 2009). Subsequently, SHOREMAP v.3.6 was used to extract SNPs and to visualize their allele frequencies (AF) (Schneeberger *et al.*, 2009; Sun & Schneeberger, 2015). SNPs having a quality

score lower than 40 were filtered out. In addition, homozygous SNPs in the *pep1-1* resequencing data were used for background correction and also subtracted from the sequencing data of the mutants (BioProject PRJNA607995).

For fine mapping of the *eop002* mutant, 12 molecular markers were developed based on the SNPs detected by the resequencing data and used to screen a total of 396 BC1F2:3 plants. Primers used for fine mapping are listed in Supporting Information Table S1. The raw sequencing data are available in BioProject under accession number PRJNA756904.

### Plasmid construction and plant transformation

For the complementation assays, we cloned *AaFRAT1* (*Aa\_G106560*) as two genomic fragments (one containing 3786 bp of its promoter and the second spanning the coding sequence and 923 bp downstream of its stop codon, comprising part of the 3' untranslated region (UTR)). Subsequently, we combined these fragments together into the GATEWAY entry vector pDONR201 (Invitrogen) using the polymerase incomplete primer extension (PIPE) method (Klock *et al.*, 2008). The resulting 6.8 kb DNA construct was sequenced and recombined into the pEarleyGate301 binary vector (Earley *et al.*, 2006). For the AaFRAT1-VENUS construct, we introduced a VENUS-tag at the C-terminal end, before the 3'UTR region. Both AaFRAT1 and AaFRAT1-VENUS constructs were transformed into the *eop085* mutant.

For the 35S::AaFRAT1 double-stranded RNA interference (dsRNAi) construct, we targeted the first exon of *AaFRAT1* (Table S1) and subsequently introduced it into the entry vector pDONR207 (Invitrogen). The fragment was then cloned into the GATEWAY-compatible vector pJawohl8-RNAi (GenBank accession number AF408413) and transformed into the *pep1-1* mutant.

*atfrat1* (*AT5G17760*) mutant alleles in *A. thaliana* were generated by the CRISPR/Cas9 method as previously described (Wang *et al.*, 2015). Potential target sites (5'-N<sub>20</sub>NGG-3') within the coding sequence of the gene and possible off-targets were identified using CCTOP (Stemmer *et al.*, 2015). The selected single guide RNA (sgRNA) target sites of *AT5G17760* were cloned into the pHEE401E vector and subsequently transformed into Col-0.

Plant transformation in *A. alpina* and *A. thaliana* was performed using the *Agrobacterium*-mediated floral dip method (Clough & Bent, 1998). All data presented originated from T3 homozygous lines carrying a single T-DNA insertion. For the *atfrat1* CRISPR lines, only T3 plants that contained editions at *AT5G17760* and lacked the *Cas9* cassette were selected. In *atfrat1* CRISPR lines, predicted off-target sequences were amplified by PCR and sequenced, to confirm that no other mutation had been introduced in the genome.

All primers used in this study are listed in Table S1.

### RNA isolation and qRT-PCR analysis

Total plant RNA was isolated using the RNeasy<sup>®</sup> Plant Mini Kit (Qiagen), followed by a DNase treatment with Ambion DNase-free<sup>™</sup> DNase Treatment and Removal kit (Invitrogen) to remove any traces of DNA contamination. One microgram total RNA

was used to synthesize cDNA through reverse transcription with the SuperScript II Reverse Transcriptase (Invitrogen) and oligo dT (18) as a primer. Two microlitres of a cDNA dilution (1 : 10) were used as a template for each reaction. Quantitative reverse transcriptase PCR (qRT-PCR) was performed using a CFX384 Real-Time System (Bio-Rad) and the iQ SYBR Green Supermix (Bio-Rad) detection system. Normalization of expression data in *A. alpina* samples was done using *AaRAN3*, *AaPP2A* and *AaUBQ10* (Stephan *et al.*, 2019), while in *A. thaliana* *AtUBC21* and *AtPP2A* were used (Czechowski *et al.*, 2005). Relative expression of target genes was calculated using the ddCT method (Livak & Schmittgen, 2001).

### Synteny and phylogenetic analysis

Synteny between *A. alpina* and *A. thaliana* *FRAT1* loci was analysed using GATA v.0.7 (Nix & Eisen, 2005). For the phylogenetic tree, amino acid sequences of members from the AAA<sup>+</sup> ATPase family in *A. thaliana* were obtained from TAIR (Berardini *et al.*, 2015) and subsequently aligned in MEGA 7.0 (Kumar *et al.*, 2016) using MUSCLE (Edgar, 2004). Using these sequences, a maximum-likelihood tree was constructed in MEGA 7.0 (LG model, 600 rounds of bootstrapping) and visualized using iTOL v.4.0 (Letunic & Bork, 2019).

### Confocal laser scanning microscopy (CLSM)

For imaging of the presence of AaFRAT1-VENUS in shoots, apices of *A. alpina* were dissected under a binocular microscope and fixed in 4% (v/v) paraformaldehyde (Sigma-Aldrich) prepared in phosphate-buffered saline at pH 7.0. Samples were vacuum-infiltrated twice for 10 min each and transferred to fresh 4% paraformaldehyde at 4°C overnight. Samples were then cleared with CLEARSEE (Kurihara *et al.*, 2015) for 4 d and the cell wall was imaged using 0.1% (v/v) SCRi Renaissance 2200 (Renaissance Chemicals, Selby, UK; Musielak *et al.*, 2016). In 10-d-old seedlings, roots were fixed in 4% (v/v) paraformaldehyde and cleared using PEA-CLARITY as described in Palmer *et al.* (2015) with slight modifications and using 50% 2,2'-thiodiethanol in 50 mM Tris buffer pH 9.5 as the final mounting medium (Musielak *et al.*, 2016). Cleared root samples were imaged with an SP8 Dive (Leica Microsystems, Wetzlar, Germany) in multiphoton mode using 965 nm light for excitation and 505–580 nm as the emission window for VENUS and 600–750 nm for autofluorescence. Cleared shoot samples were imaged with an SP8 (Leica Microsystems) using settings optimized to visualize VENUS (excitation wavelength: 514 nm; detection wavelength: 517–569 nm) and Renaissance 2200 (excitation wavelength: 405 nm; detection wavelength: 410–510 nm). Image optimization was done with IMAGEJ (Schindelin *et al.*, 2012).

### High-pressure freezing, freeze substitution and resin embedding

For transmission electron microscopy, primary and secondary *A. alpina* root tips (2 mm segments) from 10-d-old seedlings were



dissected and placed in 200 µm deep aluminium specimen carriers filled with liquid MS medium, capped with a second specimen carrier previously dipped in 1-hexadecene (flat side towards the sample) and immediately frozen using a Leica EM HPM 100 high-pressure freezer (Leica Microsystems). Freeze-substitution in 0.5% (w/v) uranyl acetate in acetone was performed in a Leica EM AFS2 freeze substitution device (Leica Microsystems) according to the protocol described in Micali *et al.* (2011). At the end of the freeze substitution run, aluminium specimen carriers were transferred to ethanol, samples were removed from the carriers and gradually infiltrated in LR White resin (Plano GmbH, Wetzlar, Germany) at  $-20^{\circ}\text{C}$  over 6 d. Resin polymerization in flat aluminium dishes covered by Aclar<sup>®</sup>-fluoropolymer film with UV light was performed for 24 h at  $-20^{\circ}\text{C}$  followed by 24 h at  $0^{\circ}\text{C}$  in the Leica EM AFS2 chamber.

#### Ultramicrotomy, IGL and transmission electron microscopy (TEM)

Ultrathin (70–90 nm) sections were produced using a PowerTome PTPC (RMC Boeckeler, Tucson, AZ, USA) and collected on nickel slot grids as described by Moran & Rowley (1987). For immunogold labelling (IGL), sections were blocked for 30 min in a 1 : 20 dilution of goat normal serum in Tris buffer (20 mM Tris, 15 mM  $\text{NaN}_3$ , 225 mM NaCl, pH 6.9) supplemented with 1% (w/v) BSA and 1% cold water fish gelatin (Tris-BSA-FG). After three washes for 10 min in Tris-BSA-FG, sections were incubated in primary antibody (overnight at  $4^{\circ}\text{C}$  or 1 h at room temperature). To detect VENUS, a 1 : 5 dilution of the rat monoclonal anti-green fluorescent protein (anti-GFP) antibody 3H9 was used (chromotek, Planegg, Germany); peroxisomes were identified by a rabbit polyclonal anti-catalase antibody (Agriseria As09 501, diluted 1 : 500; Vännäs, Sweden). After primary antibody incubation and washing in Tris-BSA-FG (four times, 10 min each), sections were incubated with a 1 : 20 dilution of the corresponding secondary antibody (goat anti-rat or goat anti-rabbit) conjugated to 10 nm colloidal gold particles (British Biocell International, Cardiff, UK) for 1 h. For double-immunogold labelling, 3H9 was detected by goat anti-rat antibodies coupled to 6 nm gold particles (Aurion, Belfast, UK). The two primary antibodies as well as the two secondary antibodies were incubated simultaneously; all other steps were as described for single labelling.

After IGL, sections were stained with 0.1% potassium permanganate in 0.1 N  $\text{H}_2\text{SO}_4$  (Sawaguchi *et al.*, 2001), followed by 2% (w/v) aqueous uranyl acetate for 10 min. Micrographs were taken with a Hitachi H-7650 transmission electron microscope (Hitachi High-Technologies Europe GmbH, Krefeld, Germany) operating at 100 kV fitted with an AMT XR41-M digital camera (Advanced Microscopy Techniques).

To facilitate recognition of gold particles on transmission electron micrographs, a colour code was added using IMAGEJ (Schindelin *et al.*, 2012). Briefly, after background subtraction, gold particles were selected by adjusting image threshold and a corresponding mask was created from the resulting selection. For double IGL, selected gold particles were sorted based on their size into two

separate masks and colour-coded accordingly. For better visibility, selected pixels of one or both masks were dilated before colour-coding. Finally, the resulting colour-coded masks were superimposed onto the original transmission electron micrograph.

**Accession numbers** AaFRAT1 (Aa\_G106560); AaFRAT2 (Aa\_G106570); PEP1 (Aa\_G579940); AaAP1 (Aa\_G283230); AaFUL (Aa\_G837900); AaLFY (Aa\_G61540); AaRAN3 (Aa\_G442020); AaPP2A (Aa\_G510870); AaUBQ10 (Aa\_G41880); AtFRAT1 (AT5G17760); AtFRAT2 (AT5G17730); AtFRAT3 (AT5G17750); AtFRAT4 (AT5G17740); DAA1 (AT1G64110); FIGL1 (AT3G27120); KTN1 (AT1G80350); RPT2A (AT4G29040); RPT4A (AT5G43010); RPT5B (AT1G09100); SKD1 (AT2G27600); PEX1 (AT5G08470); PEX6 (AT1G03000); CDC48A (AT3G09840); CDC48B (AT2G03670); CDC48C (AT5G03340); ARC1 (AT4G23940); FTSH4 (AT2G26140); FTSH5 (AT5G42270); ASD (AT5G40010); ATOM66 (AT3G50930); AtUBC21 (AT5G25760); AtPP2A (AT1G13320).

## Results

### An AAA<sup>+</sup> ATPase represses flowering in *A. alpina*

To identify floral repressors in *A. alpina* that regulate flowering in parallel with *PEP1*, we previously performed an enhancer screen in *pep1-1* (Zhou *et al.*, 2021). From the resulting mutant population, we selected and characterized three enhancer mutants (*eop002*, *eop085* and *eop091*) which flowered earlier than *pep1-1* under both LD and SD glasshouse conditions (Fig. 1a–c). The acceleration of flowering was much stronger, however, under LD than under SD. To identify the causal mutations responsible for the early flowering mutant phenotypes, we used a mapping-by-sequencing approach (Fig. S1; Tables S2–S4). In all three mutants, SHOREMAP indicated that the causal mutations mapped to a broad region on *A. alpina* chromosome 8 (Chr. 8) (Fig. S1; Tables S2–S4).  $F_1$ s generated by crossing the three mutants reciprocally did not restore the flowering phenotype of the *pep1-1* mutant, suggesting that *eop002*, *eop085* and *eop091* are allelic (Fig. S2). Interestingly, none of the mapping intervals identified from each SHOREMAP analysis carried an SNP in a previously characterized flowering time gene (Tables S1–S4). We fine-mapped the causal mutation in one of these mutants, *eop002*. We first screened 220 *eop002*BC1F2 plants and mapped the causal mutation between markers M1 and M5 (between positions 9313 334 and 18 145 960 bp in Chr.8) (Fig. S3). We subsequently narrowed down the mapping interval between markers M10 and M12 (spanning 2.45 Mb, between 14 257 447 and 16 713 521 bp in Chr. 8) by screening 176  $F_3$  seedlings from selected BC1F2 individuals (Fig. S3). In this region, a single gene (*Aa\_G106560*) predicted to encode an uncharacterized AAA<sup>+</sup> ATPase carried an SNP causing a nonsynonymous amino acid substitution (Table S2). Interestingly, *Aa\_G106560* was the only gene in this interval that carried independent SNPs in the three mutants we analysed using SHOREMAP (Fig. 1d,e; Tables S2–S4). Resequencing of the *Aa\_G106560* locus in other *eop* mutants revealed that 11 of them (*eop005*, *047*, *061*, *076*, *078*, *081*, *083*,

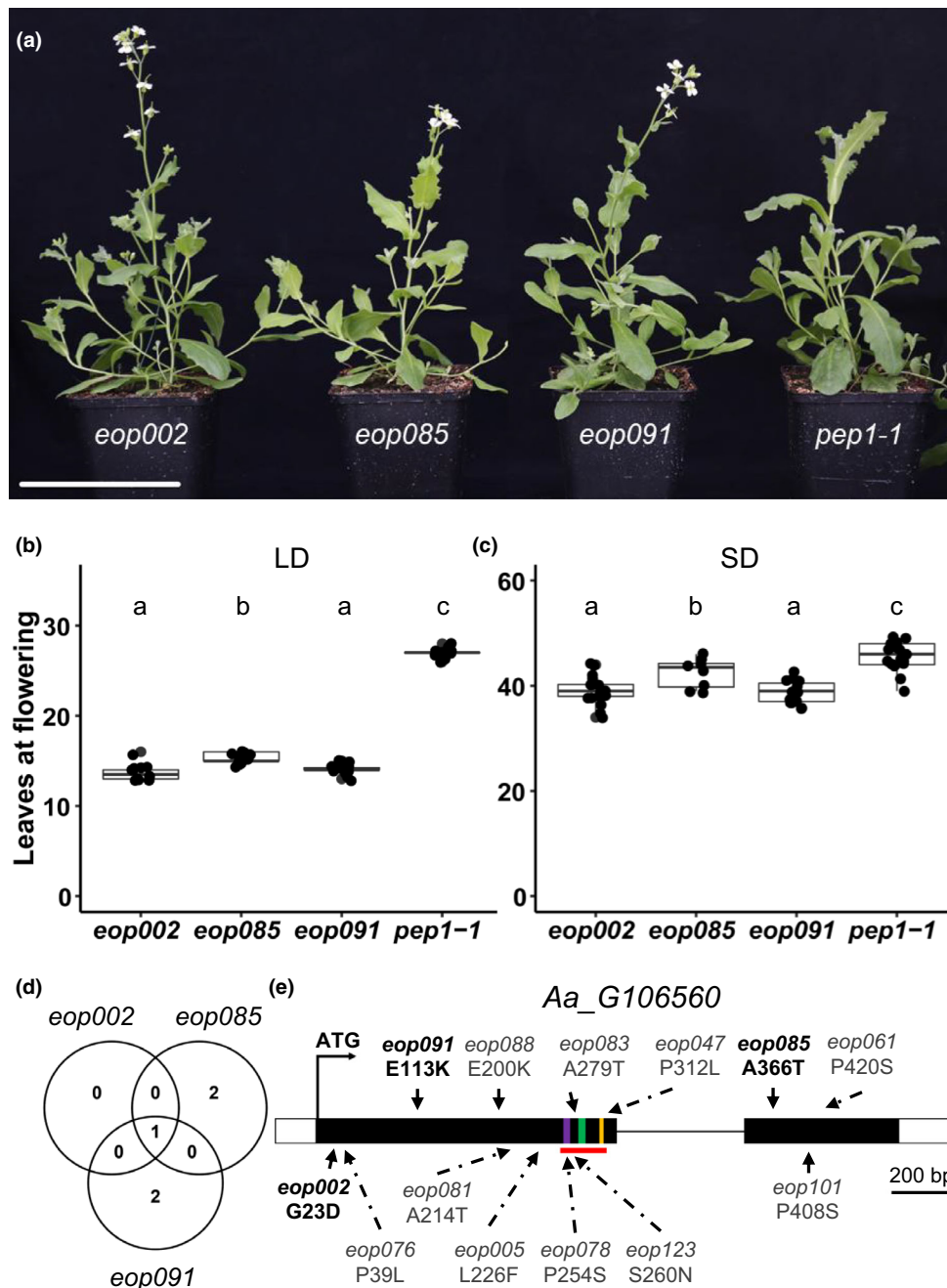


**Fig. 1** *Arabis alpina* *eop* mutants flower earlier than *pep1-1* and carry lesions in *Aa\_G106560*. (a) Flowering phenotypes of the *eop002*, *eop085*, *eop091* and *pep1-1* mutants grown for 55 d under long day (LD) conditions without vernalization. Bar, 10 cm. (b, c) Flowering time of *eop* mutants in comparison to *pep1-1* when grown either under LDs (b) or short days (SDs) (c), as determined by their total leaf number when the first flower opened. Different letters on the plots represent statistically significant differences as determined by a two-tailed ANOVA followed by Tukey's HSD *post hoc* test ( $P \leq 0.05$ );  $n \geq 12$  plants. Boxes indicate the interquartile range (IQR). The horizontal bold line in the middle represents the median of the data distribution. The vertical lines (whiskers) correspond to the maximum or minimum value within  $1.5 \times$  IQR, whereas the dots are the sample values. (d) Venn diagram showing the detected SNPs within a gene coding sequence in the reduced mapping interval between markers M10 and M12 in all three mutants. (e) Gene structure of locus *Aa\_G106560*. White boxes represent untranslated regions (UTR) and black boxes represent exons, whereas a black line represents an intron. An arrow with ATG indicates the start codon. A red line indicates the position of the ATPase domain and, within it, the Walker A (purple), Walker B (green) and arginine finger (orange) domains are shown. All identified SNPs in the *eop* mutant collection are indicated. The three mutants described in this study are indicated in bold.

087, 088, 101 and 123) also carried SNPs in the *Aa\_G106560* coding sequence, introducing nonsynonymous amino acid changes (Fig. 1e). However, none of these SNPs in *Aa\_G106560*

introduced a premature STOP codon and, with the exception of the *eop078* allele, the detected SNPs did not cause amino acid substitutions at conserved residues (Fig. 1e).

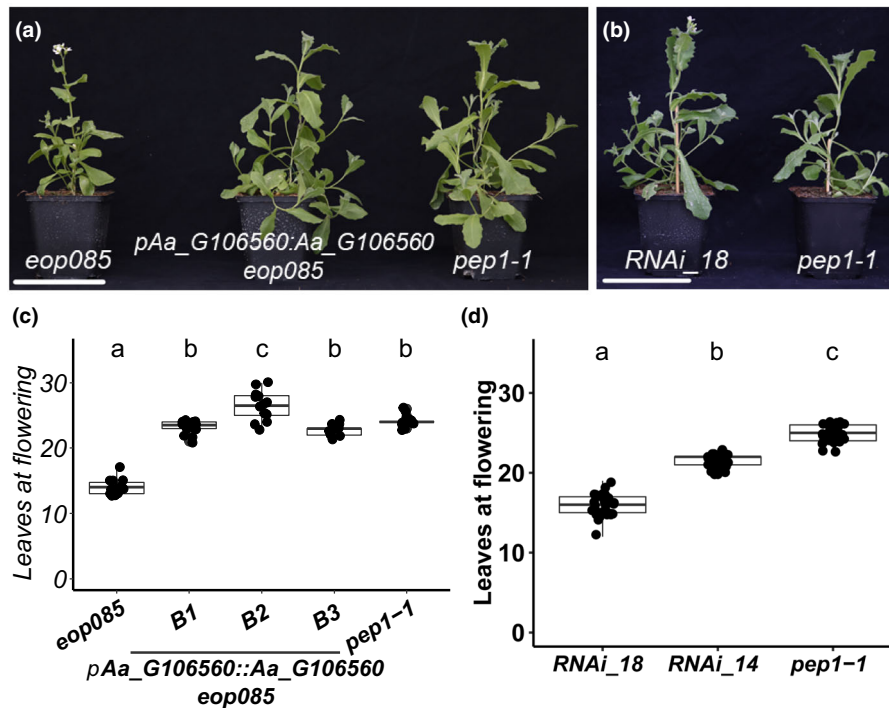


**Fig. 2** The *Arabidopsis thaliana* gene *Aa\_G106560* complements the *eop085* early flowering mutant phenotype. (a) Flowering phenotype of three T3 homozygous transgenic lines transformed with *pAa\_G106560::Aa\_G106560* (in *eop085* background) compared to *eop085* and *pep1-1* controls, grown for 52 d under long day (LD) conditions without vernalization. (b) Flowering phenotypes of *pep1-1* and the dsRNAi transgenic line #18 when grown for 50 d under LD without vernalization. Bar, 10 cm. (c) Flowering time of three independent *pAa\_G106560::Aa\_G106560* transgenic lines in comparison to *pep1-1* and *eop085* controls when grown under LDs, as determined by their total leaf number when the first flower opened;  $n \geq 12$  plants. (d) Flowering time of two independent dsRNAi transgenic lines in comparison to *pep1-1* mutant when grown under LD, as determined by their total leaf number when the first flower opened. Boxes indicate the interquartile range (IQR). The horizontal bold line in the middle represents the median of the data distribution. The vertical lines (whiskers) correspond to the maximum or minimum value within  $1.5 \times$  IQR, whereas the dots are the sample values. Different letters on the plots represent statistically significant differences as determined by a two-tailed ANOVA followed by Tukey's HSD *post hoc* test ( $P \leq 0.05$ );  $n \geq 20$  plants.

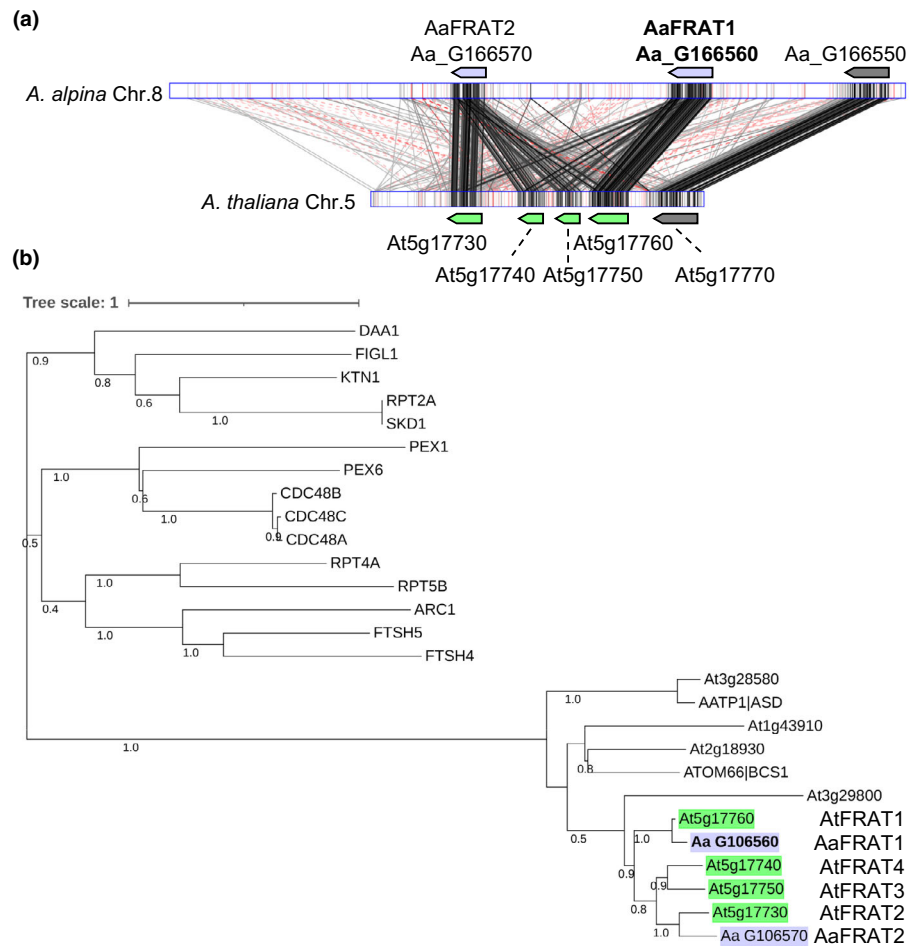
To test whether the SNPs in *Aa\_G106560* were responsible for the early flowering phenotype of these mutants, we transformed the early flowering *eop085* mutant using a 6801 bp genomic fragment, harbouring 3653 bp of the native promoter and the *Aa\_G106560* genomic fragment, including 923 bp of its 3'UTR. In these transgenic lines, the flowering phenotype of the *eop085* mutant was complemented and transgenic lines flowered as late as the *pep1-1* mutant (Fig. 2a,c). In addition, we generated transgenic plants with *Aa\_G106560* mRNA levels reduced by RNAi. Lines 14 and 18 flowered earlier than *pep1-1*, and transcript accumulation of *Aa\_G106560* in these lines correlated with their earlier flowering phenotype (Figs 2b,d, S4). Together, these results suggest that lesions in *Aa\_G106560* correlate with early flowering.

*AaFRAT1* is a member of a tandemly duplicated cluster of AAA<sup>+</sup> ATPases and has a weak flowering phenotype in *A. thaliana*

*Aa\_G106560* encodes a protein of 496 amino acids from the AAA<sup>+</sup> superfamily of ATPases, which usually present three conserved domains, namely Walker A, Walker B and an Arginine finger (Erzberger & Berger, 2006; Wendler *et al.*, 2012; Khan

*et al.*, 2021). The *A. thaliana* genome contains *c.* 140 AAA<sup>+</sup> ATPases, none of which has been reported to be involved in flowering time (Ogura & Wilkinson, 2001). *Aa\_G106560* shows 88.7% amino acid identity to the *A. thaliana* uncharacterized gene *AT5G17760* on Chr. 5. We observed that synteny at the *AT5G17760* region is conserved between *A. thaliana* and *A. alpina*, suggesting that *Aa\_G106560* is the orthologue of *AT5G17760* (Fig. 3a). Considering that *AT5G17760* has not been studied in *A. thaliana*, we named *Aa\_G106560* as *FLOWERING REPRESSOR AAA<sup>+</sup>-ATPase 1* (*AaFRAT1*), and its *A. thaliana* orthologue *AtFRAT1*. In *A. alpina*, there is also one tandemly duplicated gene (*Aa\_G106570*, *AaFRAT2*) located *c.* 11 kb upstream of *Aa\_G106560* that shows 76.13% sequence similarity to *AaFRAT1* (Fig. 3a). Similarly, we also identified *AT5G17730* (*AtFRAT2*) as a direct orthologue of *AaFRAT2* in *A. thaliana*. However, in *A. thaliana* there are four tandemly duplicated genes in this region, including *AT5G17740* (*AtFRAT4*) and *AT5G17750* (*AtFRAT3*), which are located between *AtFRAT1* and *AtFRAT2* (Fig. 3a) and probably indicate a recent duplication event. To better understand the *AaFRAT1* function, we analysed its phylogenetic relationship with other members of the extended AAA<sup>+</sup> ATPase family in *A. thaliana* which either showed high sequence similarity or which had

**Fig. 3** *AaFRAT1* in *Arabis alpina* encodes a member of the AAA<sup>+</sup> family of ATPases. (a) Comparison between the genomic regions containing the AAA<sup>+</sup> ATPase clusters in *A. alpina* (top) and *Arabidopsis thaliana* (bottom). The grey-to-black lines represent homologue regions in +/+ direction and the light-to-dark red dashed lines indicate inversions. Line intensity represents the alignment score achieved for the alignment of the sequence pairs connected by the lines. The cluster in *A. alpina* consists of two members (light purple boxes), whereas in *A. thaliana* it is formed by four genes (green boxes). (b) Phylogenetic tree of ATPase clusters from *A. alpina* and *A. thaliana*, together with other described members of the AAA<sup>+</sup> ATPase family in Arabidopsis. Node numbers indicate bootstrap percentages after 600 bootstrap repetitions. Bar, 10% sequence divergence. DAA1, DUO1-ACTIVATED ATPase; FIGL1, FIDGETIN-LIKE1; KTN1, KATANIN1; RPT2A, 4A and 5B, REGULATORY PARTICLE AAA-ATPase 2A, 4A and 5B; SKD1, SUPPRESSOR OF K<sup>+</sup> TRANSPORT GROWTH DEFECT1; PEX1 and 6, PEROXIN1 and 6; CDC48A, B and C, CELL DIVISION CYCLE48A, B and C; ARC1, ACCUMULATION AND REPLICATION OF CHLOROPLASTS1; FTSH4 and 5, FILAMENTATION TEMPERATURE SENSITIVE H4 and 5; ASD, ATPase IN SEED DEVELOPMENT; ATOM66, OUTER MITOCHONDRIAL MEMBRANE PROTEIN OF 66 KDA.



already been described in the literature (Fig. 3b). *AaFRAT1* showed high homology to the mitochondrial AAA<sup>+</sup> ATPase AtOM66 (also named BCS1) (Fig. 3b). Interestingly, we observed that AtOM66, the mitochondrial protein ASD and FRAT proteins form a separate subclade from other ATPases (Fig. 3b), in which the canonical Walker B motif (hhhhDE) (h represents any hydrophobic amino acid) is inverted to (hhhhED), but still contains the acidic residues aspartate (D) and glutamate (E), crucial for ATPase activity (Hanson & Whiteheart, 2005) (Fig. S5a). Nevertheless, the Walker A consensus sequence GXXXXGK(T/S) (X is any amino acid) in this group, essential for ATP binding, does not differ from that of other ATPases (Fig. S5b).

To test whether *AtFRAT1* also regulates flowering in *A. thaliana*, we first looked at the tissue-specific expression patterns of *AtFRAT1-4* in public databases. Among the four tandem copies, only *AtFRAT1* is consistently expressed and its transcripts have been detected in different tissues and developmental stages (Fig. S6a). We also designed specific primers for the four genes (Table S1) and tested their expression in apices of Col-0 seedlings grown for 1–5 wk under LD. Transcript accumulation of *AtFRAT1* increased at the shoot apical meristem, suggesting that *AtFRAT1* expression may be upregulated after the floral transition (Fig. S6b). To test whether *AtFRAT1* also regulates flowering in *A. thaliana*, we developed CRISPR lines targeting

specifically *AtFRAT1* (Fig. 4a). We obtained six independent mutant alleles, among which *Atfrat1-1*, *Atfrat1-2*, *Atfrat1-3*, *Atfrat1-4* and *Atfrat1-6* contained indels that caused a premature STOP codon, whereas *Atfrat1-5* had an in-frame deletion (Fig. 4a). We analysed the flowering time of these mutant alleles under LD and SD conditions. Under LD, mutants *Atfrat1-1* to *1-4* flowered with reduced number of leaves compared to the wild-type (Fig. 4b,d). Under SD, *Atfrat1-3*, *1-5* and *1-6* showed significant differences in leaf number at flowering, but with a slight delay, rather than acceleration of flowering time (Fig. 4c,e). These results suggest that *AtFRAT1* may repress flowering in *A. thaliana* under LD conditions, but its effect is not as strong as that of *AaFRAT1* in *A. alpina*. Overall, we conclude that *AaFRAT1* is the orthologue of *AT5G17760*, it encodes an AAA<sup>+</sup> ATPase, and it acts as a floral repressor in *A. alpina* and *A. thaliana*.

**AaFRAT1 regulates the duration of vernalization required for flowering and the maintenance of vegetative growth in axillary branches**

In *A. alpina*, *AaFRAT1* is expressed in different tissues and at different developmental stages (Fig. S6c). To understand the role of *AaFRAT1* in flowering, we followed its transcript accumulation in shoot apices of wild-type plants, which require exposure to



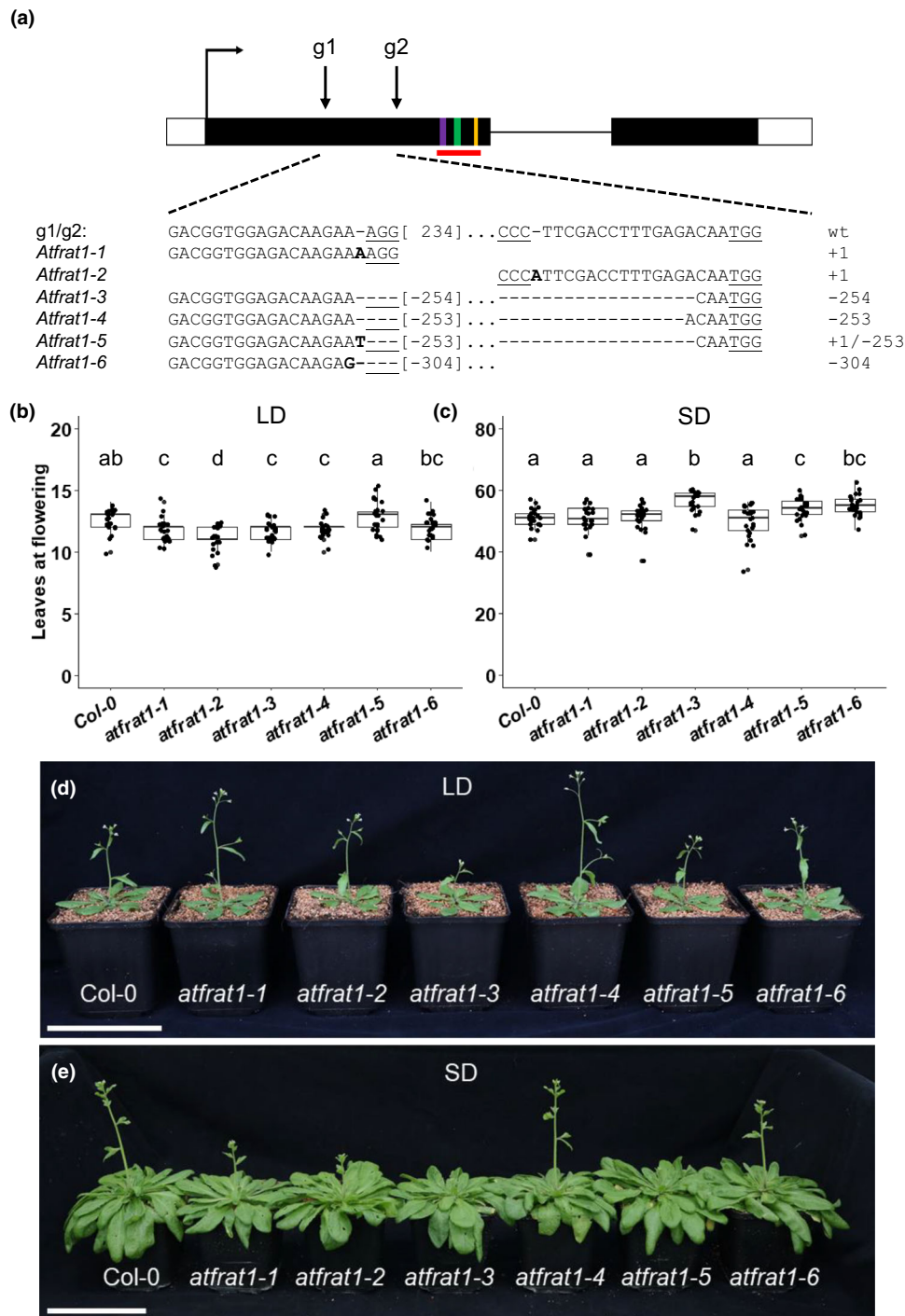


**Fig. 4** *AtFRAT1* in *Arabidopsis thaliana* plays a minor role in flowering time. (a) Summary of the *Atfrat1* mutant alleles generated by CRISPR/Cas9. Two different guides (g1 and g2) were designed within the first exon of *AT5G17760*. All alleles were confirmed by Sanger sequencing, as indicated. PAM sequences are underlined. Numbers in brackets represent the number of nucleotides between guides, or those deleted by CRISPR, when a dash precedes them. On the right-hand side, the resulting edition is shown. Gene model as described in Fig. 1e. (b, c) Flowering time of the CRISPR-induced alleles grown under long day (LD, b) or short day (SD, c) conditions, as determined by their total leaf number when the first flower opened. Boxes indicate the interquartile range (IQR). The horizontal bold line in the middle represents the median of the data distribution. The vertical lines (whiskers) correspond to the maximum or minimum value within  $1.5 \times$  IQR, whereas the dots are the sample values. Different letters on the plots represent statistically significant differences as determined by a two-tailed ANOVA followed by Tukey's HSD *post hoc* test ( $P \leq 0.05$ );  $n \geq 20$  plants. (d, e) Flowering phenotypes of the CRISPR-induced alleles grown for 21 d under LD (d) or for 57 d under SD (e). Bar, 10 cm.

prolonged cold periods (vernalization) to flower. We monitored *AaFRAT1* transcript accumulation before (5 and 8 wLD), during (1, 3, 5 and 12 wVern) and after vernalization (1, 3, 5, wLD). In

the main shoot apex, *AaFRAT1* expression was high before and during early stages of cold exposure (up to 5 wVern), and it decreased and remained low after cold (at 12 wVern and 1–3



wLD; Fig. 5a). In the same tissue, *PEP1* mRNA levels responded to cold much faster and were downregulated already after 1 wk of cold exposure (1wVern; Fig. 5b). *AaFRAT1* transcript accumulation in the shoot apices of axillary branches that maintain vegetative growth in *A. alpina* (V3; Lázaro *et al.*, 2018; Vayssières *et al.*, 2020) followed a similar pattern to that of *PEP1* (Fig. 5a,b). Specifically, after vernalization, both *AaFRAT1* and *PEP1* had high expression in apices of V3 axillary branches (V3; Fig. 5a,b) suggesting that *AaFRAT1* also contributes to the perennial growth habit by maintaining vegetative growth in these axillary branches. Interestingly, the upregulation of *AaFRAT1* expression after vernalization in the shoot apical meristem was not as strong as in the axillary branches.

To determine whether the downregulation of *AaFRAT1* mRNA levels at later stages of vernalization plays a role in the vernalization requirement in *A. alpina*, we introgressed the mutant *Aafrat1* alleles into the wild-type background. For this, we crossed the *eop002* and *eop085* alleles with Pajares and selected two introgression lines (*eop002\_IL* and *eop085\_IL*) that were homozygous for the SNPs at *AaFRAT1* while carrying a functional *PEP1*. Without vernalization, *eop002\_IL* and *eop085\_IL* behaved as Pajares and did not flower, suggesting that *AaFRAT1* cannot overcome the repressive role of *PEP1* in flowering in the absence of cold (Fig. 5c). We then exposed these genotypes to different durations of vernalization (8, 12 and 18 wVern) and observed that the *eop002\_IL* and *eop085\_IL* lines flowered faster after different durations of cold compared to the wild-type, showing the strongest phenotype after only 8 wk of cold exposure (Fig. 5d). Flowering was accelerated in the introgression lines after 8 wk of cold exposure, at which point the majority of the wild-type plants did not flower (Fig. 5d). This acceleration of flowering in the introgression lines also correlated with earlier upregulation of other floral integrators during vernalization (Fig. S7). In addition, the proportion of flowering V3 axillary branches in the IL lines was higher, whereas in the wild-type it was conditional on the duration of vernalization applied (Fig. 5e). Flowering in the V3 branches in the introgression lines was correlated with increased transcript accumulation of *AaFUL*, *AaLFY* and *AaAPI* after vernalization. Interestingly, in this tissue, the upregulation of *PEP1* mRNA levels after vernalization was reduced compared to the wild-type. These results suggest that *AaFRAT1* affects the duration of vernalization required for flowering and contributes to the maintenance of vegetative development, potentially through *PEP1*.

### *AaFRAT1* is localized at the interphase between the ER and peroxisomes

To gain insights into the function of *AaFRAT1*, we investigated its accumulation patterns and localization *in planta*. For this, we complemented the *eop085* mutant with a genomic fragment carrying the *AaFRAT1* locus and a VENUS-tag fused to the C-terminus (*AaFRAT1*-VENUS) (Fig. S8). In vegetative apices of plants grown under LD conditions, we detected most *AaFRAT1*-VENUS in leaf primordia (Fig. 6a–c), whereas in apices that had already transitioned to flowering, the protein accumulated mostly

below the meristem and in floral primordia (Fig. 6d–f). *AaFRAT1* protein localization showed a similar pattern in apices of cold-treated plants, regardless of whether plants had transitioned to flowering or not (Fig. S9).

In seedling roots, *AaFRAT1*-VENUS was abundant in pericycle cells and, to a lesser extent, in the cortex and endodermis cells (Fig. 6g–i). While the signal in the cortex and endodermis appeared to be associated with the cell periphery in the meristematic and elongation zones (Fig. 6k), only a punctuate cytosolic pattern was visible in older parts of the root cortex and in the pericycle (Fig. 6j,k), resembling that observed in leaf primordia (inset in Fig. 6a).

AAA<sup>+</sup> ATPases are localized in different compartments of the cell (White & Lauring, 2007). To analyse the subcellular localization of *AaFRAT1*-VENUS, we used IGL coupled with TEM in roots of two *AaFRAT1*-VENUS transgenic lines (2.1.3 and 2.1.6). Using anti-GFP antibodies to detect VENUS, we observed a very distinct signal at specific subcellular locations with very little background elsewhere in the cell (Fig. 7a–c; yellow; Fig. S10). The signal was found at the rim of homogeneously electron-dense, ribosome-free organelles of fine granular appearance which were devoid of any obvious internal membranes (stars in Fig. 7a–c). In primary roots, these organelles frequently contained elongated, paracrystalline inclusions (arrowheads in Fig. 7c). These features as well as the punctate labelling pattern observed by CLSM suggested that the structures detected by anti-GFP antibodies were peroxisomes. This was further confirmed using a double labelling approach (anti-catalase antibody as peroxisomal marker and anti-GFP antibody to detect *AaFRAT1*-VENUS with gold-conjugated secondary antibody in blue and yellow, respectively; Fig. 7d–g). *AaFRAT1*-VENUS protein localization was similar in primary (Fig. 7a–c,e–g) and lateral roots (Fig. 7b,e) and showed a similar pattern in both transgenic lines analysed (Fig. 7a–e for line 2.1.6; Fig. 7f,g for line 2.1.3). Near the labelled peroxisomes, an abundance of ER tubules was frequently observed (arrows in Fig. 7), characterized by their electron-translucent content and by linear or spirally arranged ribosomes on their surface. When section orientation was perpendicular to the ER-peroxisome interface, IGL of *AaFRAT1*-VENUS epitopes was aligned along this interface (Figs 7b,c,e, S11).

The specific localization shown by IGL of *AaFRAT1*-VENUS at the ER–peroxisomal interface suggests that *AaFRAT1* may be involved in ER–peroxisome tethering or in protein transport between these organelles (either directly or vesicle-mediated). Mutants affected in peroxisomal activity usually show defects in seedling growth and development, due to reduced supply of carbohydrates derived from  $\beta$ -oxidation of fatty acids (Kao *et al.*, 2018), as well as insensitivity to the presence of auxin precursors, which are also processed by  $\beta$ -oxidation. To rule out any possible effect of *AaFRAT1* on peroxisomal activity, we tested whether the *AaFRAT1*-VENUS lines showed any peroxisomal phenotypes by measuring hypocotyl elongation in the dark, in both the presence and absence of sucrose, as well as in the presence of the auxin precursor indole-3-butyric acid (IBA; Fig. S12a). In all three conditions, we observed that the *eop085* mutant seems to elongate slightly more than *pep1-1*. *AaFRAT1*-VENUS

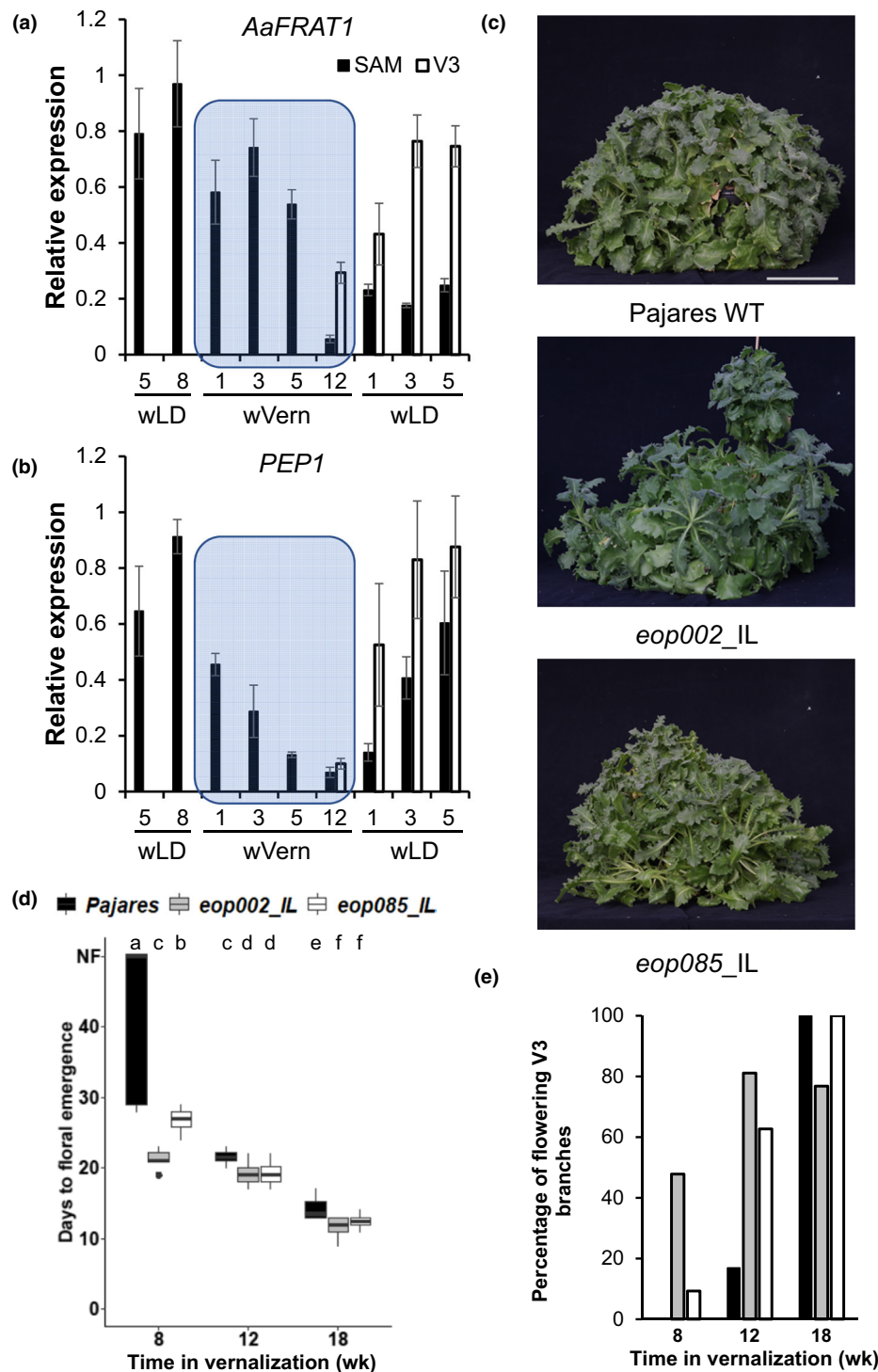


**Fig. 5** *AaFRAT1* in *Arabis alpina* contributes to the duration of vernalization required for flowering. (a, b) Relative expression of *AaFRAT1* (a) and *PEP1* (b) in main apices and V3 axillary buds of wild-type *A. alpina* plants at different stages during development. The blue boxes represent the period during which plants were exposed to vernalization (4°C and short days (SD)). Bar plots represent the average of three biological replicates. Error bars represent standard deviation. (c) Phenotype of Pajares wild-type (WT), *eop002\_IL* and *eop085\_IL* lines grown for 126 d under long days (LDs) without vernalization. Bar, 10 cm. (d) Time required for floral emergence after different durations of vernalization. Boxes indicate the interquartile range (IQR). The horizontal bold line in the middle represents the median of the data distribution. The vertical lines (whiskers) correspond to the maximum or minimum value within 1.5 × IQR, whereas the dots are the sample values. Different letters on the plot represent statistically significant differences as determined by a two-tailed ANOVA followed by Tukey's HSD *post hoc* test ( $P \leq 0.05$ ). NF, not flowered. (e) Effect of different lengths of vernalization on the flowering behaviour of V3 branches. Colours correspond to the same genotypes as in (d). Error bars represent standard deviation;  $n = 12$  plants.



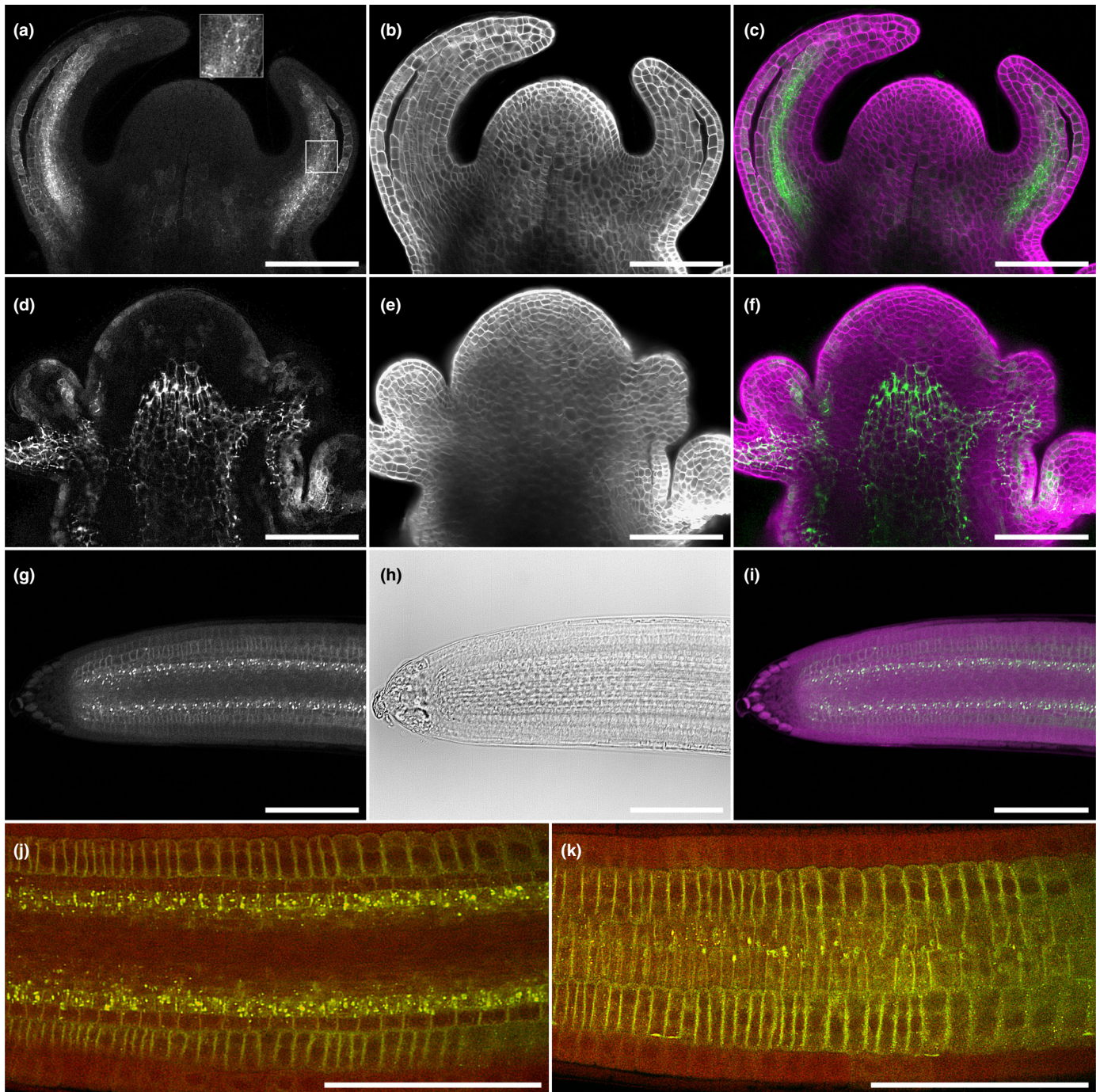


**Fig. 6** AaFRAT1-VENUS accumulation patterns change during development and between tissues in *Arabis alpina*. (a–f) Confocal imaging of fixed apices of *pAaFRAT1::AaFRAT1-VENUS* T3 transgenic lines (*eop085* mutant background, line 2.1.6) at the vegetative stage (5 wLD) (a–c) and after the transition to flowering occurred (11 wLD) (d–f). From left to right, panels show the VENUS signal (a, d), Renaissance 2200 staining of cell walls (b, e), and the merged signal of VENUS (green) and Renaissance 2200 (magenta) (c, f). (g–k) Confocal imaging of roots from 10-d-old *pAaFRAT1::AaFRAT1-VENUS* T3 transgenic seedlings (*eop085* mutant background, line 2.1.6). From left to right, panels show the VENUS signal (g), bright field (h), and the merged signal of VENUS (green) and bright field (magenta) (i). (j, k) Details of the root showing the punctuate pattern of the signal in the pericycle (j) and the transition from cell periphery-associated puncti to cytosolic puncti in the root cortex (k). Red colour corresponds to autofluorescence signal. Bar, 100  $\mu$ m.

transgenic lines also showed hypocotyl elongation, suggesting that there is not a clear correlation of AaFRAT1 with peroxisomal activity. In *Arabidopsis*, the observed differences were also very mild, suggesting that AtFRAT1 does not compromise peroxisomal activity (Fig. S12b).

Taken together, we have observed that AaFRAT1 accumulation is dynamic, changing from leaf primordia in vegetative apices to the rib zone under the meristem once the flowering transition has occurred. At the subcellular level, we confirmed that AaFRAT1 is closely associated with ER tubules and



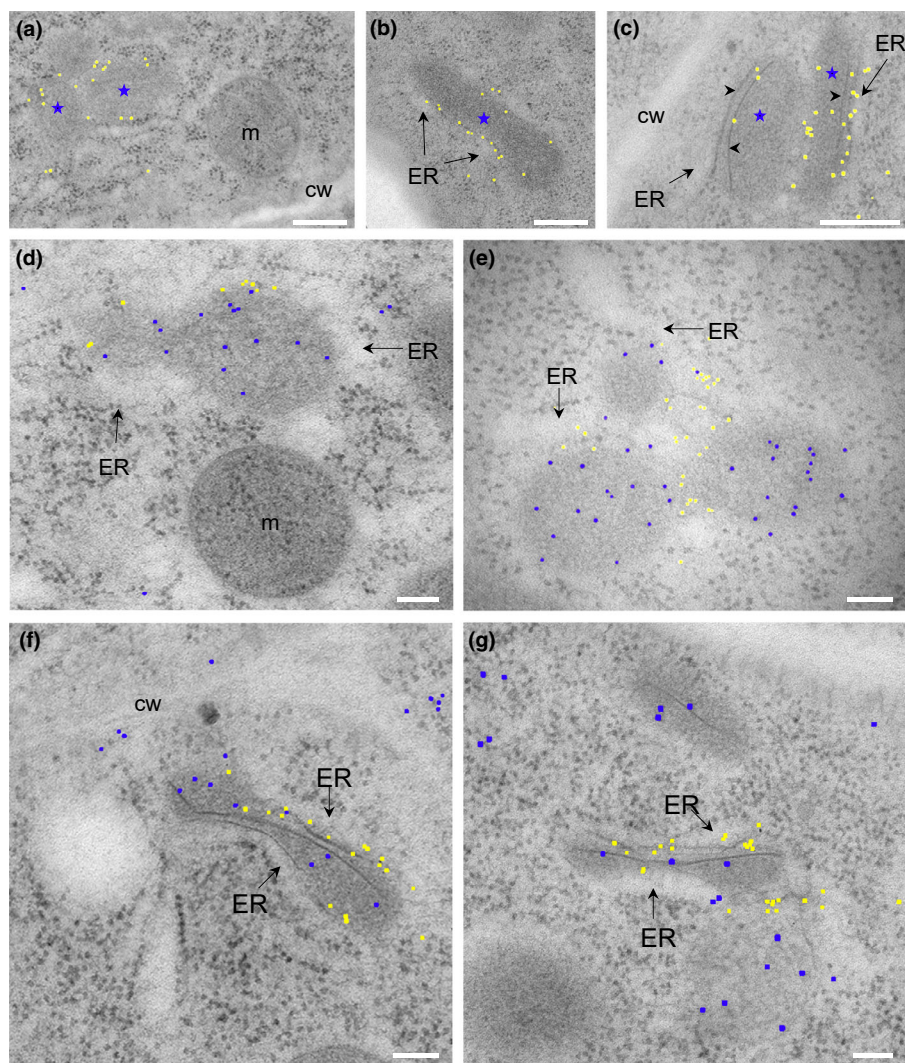


**Fig. 7** AaFRAT1-VENUS in *Arabis alpina* locates to the interphase between the ER and peroxisomes. (a, b) Primary roots (line 2.1.6) showing single immunogold labelling (IGL) of AaFRAT1-VENUS (yellow pseudocolour) at specific subcellular locations in close proximity to ER tubules. Stars indicate organelles that contain paracrystalline inclusions (arrowheads in c), probably peroxisomes. (d–g) Primary (d) and secondary (e) roots (line 2.1.6) showing double IGL of AaFRAT1-VENUS (yellow pseudocolour) and of catalase, a peroxisomal marker (blue pseudocolour). (f–g) Primary (f) and secondary (g) roots (line 2.1.3) showing double IGL of AaFRAT1-VENUS (yellow pseudocolour) and of catalase, a peroxisomal marker (blue pseudocolour). cw, cell wall; ER, endoplasmic reticulum; m, mitochondria. Bars: (a–c) 250  $\mu\text{m}$ ; (d–g) 100  $\mu\text{m}$ .

peroxisomes, usually located at contact sites between them. However, we have no clear evidence to support that AaFRAT1 affects peroxisomal activity.

## Discussion

AAA<sup>+</sup> ATPases are present in all eukaryotes, acting as macromolecular machines powered by the energy derived from ATP hydrolysis to induce conformational changes in their substrates (White & Lauring, 2007). While their core ATPase module is structurally highly conserved (Erzberger & Berger, 2006; Khan *et al.*, 2021), the remaining regions of these proteins are quite variable and show great diversity, which accounts for their multiple functions and roles (Snider *et al.*, 2008). AAA<sup>+</sup> ATPases are molecular chaperones that affect the fate of other proteins by facilitating protein folding and unfolding, the assembly or disassembly of protein complexes, aiding membrane fusion events, unwinding of DNA, altering DNA–protein complexes or participating in protein degradation (Ogura & Wilkinson, 2001). In plants, some ATPase null mutants are embryo lethal, due to their role in embryo development (Park *et al.*, 2008; Muralla *et al.*,

2011; Li *et al.*, 2019a). Similar to what is known in other species, some plant ATPases participate in intracellular transport and vesicle trafficking, such as SUPPRESSOR OF K<sup>+</sup> TRANSPORT GROWTH DEFECT 1 (SKD1) or N-ETHYLMALIMIDE SENSITIVE FACTOR (AtNSF) (Shahriari *et al.*, 2010; Reyes *et al.*, 2014; Tang *et al.*, 2021), or in the degradation of ubiquitinated substrates via the 26S proteasome (Bar-Nun & Glickman, 2012; Yedidi *et al.*, 2017). Moreover, many members of this family have been shown to participate in immune responses and defence from pathogens (Sugimoto *et al.*, 2004; Lee & Sano, 2007; Zhang *et al.*, 2014; Zhu *et al.*, 2016; Liu *et al.*, 2020). In plant development, several AAA<sup>+</sup> ATPases were shown to participate in male meiosis and pollen formation (Girard *et al.*, 2015; Zhang *et al.*, 2017), pollen tube development (Riglet *et al.*, 2020), as well as seed development (Baek *et al.*, 2011) and germination (Li *et al.*, 2019b). AAA<sup>+</sup> ATPases also contribute to the regulation of developmental progress and growth, such as root meristem maintenance, for example by regulating the pattern of auxin maxima in the embryo, which will give rise to the root apical meristem (Li *et al.*, 2019a); by ensuring a normal developmental pattern and cell growth (Bae *et al.*, 2009); by



preventing early meristem termination as a result of reactive oxygen species (ROS) accumulation (Dolzblasz *et al.*, 2016); or by ensuring the correct timing of programmed proteolysis at the meristems (Ueda *et al.*, 2004). The role of AAA<sup>+</sup> ATPases in the regulation of flowering time has not yet been described, although mutants in the mitochondrial metalloprotease AtFtsH4 showed late flowering in addition to other developmental defects compared to the wild-type, probably caused by ROS imbalances (Gibala *et al.*, 2009).

In this study we identified and characterized *AaFRAT1*, an AAA<sup>+</sup> ATPase that is involved in the regulation of flowering in *A. alpina*. Although our data do not provide a direct link between the AAA<sup>+</sup> ATPase and flowering, the fact that *Aafrat1* mutants do not show pleiotropic phenotypes suggests that the main role of AaFRAT1 lies within the flowering pathway. Nevertheless, among the detected 14 *Aafrat1* mutant alleles, none caused a premature STOP codon. This result suggests that null *Aafrat1* alleles may be lethal and therefore were not detected in the original mutant population. Conversely, in *A. thaliana*, AtFRAT1 does not seem to play a major developmental role, as CRISPR lines carrying mutated variants of the AtFRAT1 protein only showed subtle phenotypes. The lack of a strong flowering phenotype in the *Aafrat1* CRISPR mutants could result from functional redundancy with the other AAA<sup>+</sup> ATPases in the cluster. This, however, is not evident from our data because we did not detect transcript accumulation of *AtFRAT2-4* in the tissues we tested. As it might still be possible that *AtFRAT2-4* compensate for the loss of function of AtFRAT1 in the CRISPR lines, protein abundance and stability of these AAA<sup>+</sup> ATPases should be examined. The flowering phenotype in the *Aafrat1* mutants could also be influenced by the background used to create the CRISPR lines. Col-0 is a rapid-cycling accession and does not require vernalization to accelerate flowering. Thus, it would be interesting to test the effect of our CRISPR *afrat1* alleles in accessions, such as Lov-1, that have a strong requirement for vernalization to flower (Duncan *et al.*, 2015).

Similar to other regulators of flowering previously described in *A. alpina*, AaFRAT1 also contributes to other traits related to flowering. Specifically, the length of the vernalization exposure required for the plants to flower and the proportion of axillary branches that maintain vegetative growth after flowering were both affected by AaFRAT1. The fact that *frat1* mutants were isolated in an enhancer screen using *pep1-1* as background (Zhou *et al.*, 2021) suggests that AaFRAT1 acts in parallel to PEP1 and may or may not directly participate in the vernalization pathway. Nevertheless, the low recovery of *PEP1* transcript accumulation in the axillary branches suggests that AaFRAT1 may play two distinct roles: first, before and during vernalization, by repressing flowering in parallel of PEP1; and second, after vernalization, to keep *PEP1* expression low in axillary branches and ensure the maintenance of vegetative growth. The specific molecular relationship between AaFRAT1 and PEP1, however, still needs to be determined.

Our experiments also showed that *AaFRAT1* expression is reduced upon prolonged periods of cold and that AaFRAT1 protein localization seems to be influenced by cold exposure.

Moreover, in the absence of cold, AaFRAT1 protein accumulation changed following the developmental stage of the meristem. The meaning of these observations is not yet clear, although it might be indicative that once the protein has completed its role, it becomes deactivated/stored in the cell periphery or that it responds to certain stimuli. Interestingly, the effect of development on AaFRAT1 dynamics and distribution was suppressed by application of cold treatment, which might indicate that the function of AaFRAT1 is modified once the plant experiences vernalization. Seasonal fluctuations in temperature have been previously shown to influence protein localization and accumulation of flowering time regulators (Zhu *et al.*, 2021). Further research will be needed to determine whether the accumulation patterns we observed for AaFRAT1 somehow resemble this.

At the subcellular level, the presence of AaFRAT1 at the interphase between the ER and peroxisomes suggests that it participates either in tethering complexes, anchoring the organelle membranes; in transport processes occurring between organelles; or in the process of peroxisome biogenesis. Contact sites between the ER and peroxisomes have already been reported, usually participating in peroxisome replication or stress responses (Mullen & Trelease, 2006; Sinclair *et al.*, 2009). However, it is also important to note that our observations were made in seedling roots. Recent reports have stressed the dynamic behaviour of peroxisomal contacts with other organelles and how they change from etiolated tissues compared to photosynthetic ones (Oikawa *et al.*, 2019). Therefore, it is also possible that an evaluation of subcellular localization of AaFRAT1 in older leaves would differ from that shown by our TEM experiments.

Tethering complexes are fundamental for targeting transport vesicles within the cell, as they mediate the contact between the target's membrane and that of the vesicle (Vukašinovic & Žárský, 2016). This not only involves transport *per se*, but also ensures proper recognition of the target, a process usually carried out by groups of proteins that change depending on the cell compartments involved, but which usually include members of the soluble NSF protein attachment protein receptor (SNARE) complexes as well as ATPases, both essential for membrane fusion events during vesicle transport (Baker & Hughson, 2016; Tang *et al.*, 2021).

However, the possible connection of AaFRAT1 in vesicle transport processes with the regulation of flowering is not straightforward. The better established connection of flowering time regulation with transport processes is that of FLOWERING LOCUS T (FT), which is produced in leaves under photoperiod-inductive conditions and then transported to the shoot apical meristem through the phloem, where it triggers the floral transition (Corbesier *et al.*, 2007; Jaeger & Wigge, 2007). The specific mechanisms controlling this long-distance trafficking have started to be elucidated. Briefly, members of the family of multiple C2 domain and transmembrane region proteins (MCTPs) and SNARE proteins act coordinately to transport FT-loaded endosomal vesicles through plasmodesmata from companion cells to sieve elements, a process in which the ER is also involved (Liu *et al.*, 2019). Consequently, mutants of the transporters involved

in this process showed delayed flowering (Liu *et al.*, 2019). TFL1, a PEBP protein related to FT, has also been shown to act as a mobile transcriptional repressor both at the shoot apical meristem and seeds of *A. thaliana* (Conti & Bradley, 2007; Gortetti *et al.*, 2020; Zhang *et al.*, 2020). In this case, the transport is mediated by members of the Ran subfamily of GTPases, although the specific mechanism remains unclear (Zhang *et al.*, 2020). We speculate that AaFRAT1 may participate in such transport processes of a floral repressor or an enhancer of a floral repressor, thus influencing the flowering behaviour. This is also supported by the upregulation of genes involved at early stages of the floral transition in the introgression lines carrying *Aafrat1* alleles compared to the wild-type. AaFRAT1 function could also involve changes in chromatin structure that would result in transcriptional regulation of *PEP1*. This role, however, should be indirect, as AaFRAT1 protein is not localized in the nucleus. Thus, AaFRAT1 can be used as a stepping stone to unravel the role of AAA<sup>+</sup> ATPases in flowering and the mechanisms in which they participate.










## Acknowledgements

MCA acknowledges support from the Deutsche Forschungsgemeinschaft (DFG, German Research Foundation) under Germany's Excellence Strategy – EXC 2048/1 – Project ID: 529 390686111. The authors would like to thank Eva Madrid for critical reading of the manuscript and Imogen Sparkes for providing feedback. The authors are extremely grateful to Yan Zeng, Julia Benecke, Ila Rouhara and Anne Harzen for their technical assistance in the lab and to Margaret Kox for proofreading of the manuscript. Open Access funding enabled and organized by ProjektDEAL.

## Author contributions

NVT and MCA planned and designed the research; MCA performed the initial mutagenesis screen; NVT, AV, EO-H, UN, AL, YZ, TT, AR and SCS performed experiments; NVT, AV, EO-H, UN, AL, TT, SCS, HN and MCA analysed the data; HS and KS provided assistance with SHOREMAP analyses; NVT and MCA wrote the manuscript incorporating input and feedback from all coauthors. AV and EO-H contributed equally to this work.

## ORCID

Maria C. Albani  <https://orcid.org/0000-0002-8215-020X>  
 Hirofumi Nakagami  <https://orcid.org/0000-0003-2569-7062>  
 Ulla Neumann  <https://orcid.org/0000-0001-9200-4209>  
 Korbinian Schneeberger  <https://orcid.org/0000-0002-5512-0443>  
 Sara C. Stolze  <https://orcid.org/0000-0002-1421-9703>  
 Hequan Sun  <https://orcid.org/0000-0003-2046-2109>  
 Alice Vayssières  <https://orcid.org/0000-0002-8625-2879>  
 Natanael Viñegra de la Torre  <https://orcid.org/0000-0003-3773-6014>  
 Yanhao Zhou  <https://orcid.org/0000-0002-6009-8447>

## Data availability

The data that support the findings of this study are available from the corresponding author upon reasonable request. The sequencing data of the mutants are available in NCBI Bioproject under accession nos. PRJNA607995 and PRJNA756904.

## References

- Albani MC, Coupland G. 2010. Comparative analysis of flowering in annual and perennial plants. In: Timmermans MCP, ed. *Current topics in developmental biology*. Amsterdam, the Netherlands: Elsevier, 323–348.
- Amasino R. 2009. Floral induction and monocarpic versus polycarpic life histories. *Genome Biology* 10: 228.
- Bae H, Choi SM, Yang SW, Pai H-S, Kim WT. 2009. Suppression of the ER-localized AAA ATPase NgCDC48 inhibits tobacco growth and development. *Molecules and Cells* 28: 57–65.
- Baek K, Seo PJ, Park CM. 2011. Activation of a mitochondrial ATPase gene induces abnormal seed development in Arabidopsis. *Molecules and Cells* 31: 361–369.
- Baker RW, Hughson FM. 2016. Chaperoning SNARE assembly and disassembly. *Nature Reviews Molecular Cell Biology* 17: 465–479.
- Bar-Nun S, Glickman MH. 2012. Proteasomal AAA-ATPases: structure and function. *Biochimica et Biophysica Acta (BBA) – Molecular Cell Research* 1823: 67–82.
- Berardini TZ, Reiser L, Li D, Mezheritsky Y, Muller R, Strait E, Huala E. 2015. The arabidopsis information resource: making and mining the 'gold standard' annotated reference plant genome. *Genes* 53: 474–485.
- Bergonzi S, Albani MC, Ver Loren van Themaat E, KJV N, Wang R, Schneeberger K, Moerland PD, Coupland G. 2013. Mechanisms of age-dependent response to winter temperature in perennial flowering of *Arabis alpina*. *Science* 340: 1094–1097.
- Clough SJ, Bent AF. 1998. Floral dip: a simplified method for Agrobacterium-mediated transformation of *Arabidopsis thaliana*. *The Plant Journal* 16: 735–743.
- Conti L, Bradley D. 2007. TERMINAL FLOWER1 is a mobile signal controlling Arabidopsis architecture. *Plant Cell* 19: 767–778.
- Corbesier L, Vincent C, Jang S, Fornara F, Fan Q, Searle I, Giakountis A, Farrona S, Gissot L, Turnbull C *et al.* 2007. FT protein movement contributes to long-distance signaling in floral induction of Arabidopsis. *Science* 316: 1030–1033.
- Czechowski T, Stitt M, Altmann T, Udvardi MK, Scheible W-R. 2005. Genome-wide identification and testing of superior reference genes for transcript normalization in Arabidopsis. *Plant Physiology* 139: 5–17.
- Dolzblass A, Smakowska E, Gola EM, Sokolowska K, Kicia M, Janska H. 2016. The mitochondrial protease AtFTSH4 safeguards Arabidopsis shoot apical meristem function. *Scientific Reports* 6: 28315.
- Duncan S, Holm S, Questa J, Irwin J, Grant A, Dean C. 2015. Seasonal shift in timing of vernalization as an adaptation to extreme winter. *eLife* 4: 6620.
- Earley KW, Haag JR, Pontes O, Opper K, Juehne T, Song K, Pikaard CS. 2006. Gateway-compatible vectors for plant functional genomics and proteomics. *The Plant Journal* 45: 616–629.
- Edgar RC. 2004. MUSCLE: Multiple sequence alignment with high accuracy and high throughput. *Nucleic Acids Research* 32: 1792–1797.
- Erzberger JP, Berger JM. 2006. Evolutionary relationships and structural mechanisms of AAA<sup>+</sup> proteins. *Annual Review of Biophysics and Biomolecular Structure* 35: 93–114.
- Gibala M, Kicia M, Sakamoto W, Gola EM, Kubrakiewicz J, Smakowska E, Janska H. 2009. The lack of mitochondrial AtFtsH4 protease alters Arabidopsis leaf morphology at the late stage of rosette development under short-day photoperiod. *The Plant Journal* 59: 685–699.
- Girard C, Chelysheva L, Choinard S, Froger N, Macaisne N, Lehemdi A, Mazel J, Crismani W, Mercier R. 2015. AAA-ATPase FIDGETIN-LIKE1 and helicase FANCM antagonize meiotic crossovers by distinct mechanisms. *PLoS Genetics* 11: e1005369.

- Goretto D, Silvestre M, Collani S, Langenecker T, Méndez C, Madueño F, Schmid M. 2020. TERMINAL FLOWER1 functions as a mobile transcriptional cofactor in the shoot apical meristem. *Plant Physiology* 182: 2081–2095.
- Hanson PI, Whiteheart SW. 2005. AAA+ proteins: have engine, will work. *Nature Reviews Molecular Cell Biology* 6: 519–529.
- Hughes PW, Soppe WJJ, Albani MC. 2019. Seed traits are pleiotropically regulated by the flowering time gene PERPETUAL FLOWERING1 (PEP1) in the perennial *Arabis alpina*. *Molecular Ecology* 28: 1183–1201.
- Hyun Y, Vincent C, Tilmes V, Bergonzi S, Kiefer C, Richter R, Martinez-Gallegos R, Severing E, Coupland G. 2019. A regulatory circuit conferring varied flowering response to cold in annual and perennial plants. *Science* 363: 409–412.
- Jaeger KE, Wigge PA. 2007. FT protein acts as a long-range signal in *Arabidopsis*. *Current Biology* 17: 1050–1054.
- Jiao W-B, Accinelli GG, Hartwig B, Kiefer C, Baker D, Severing E, Willing E-M, Piednoel M, Woetzel S, Madrid-Herrero E *et al.* 2017. Improving and correcting the contiguity of long-read genome assemblies of three plant species using optical mapping and chromosome conformation capture data. *Genome Research* 27: 778–786.
- Kao YT, Gonzalez KL, Bartel B. 2018. Peroxisome function, biogenesis, and dynamics in plants. *Plant Physiology* 176: 162–177.
- Khan YA, White KI, Brunger AT. 2021. The AAA+ superfamily: a review of the structural and mechanistic principles of these molecular machines. *Critical Reviews in Biochemistry and Molecular Biology* 57: 1–32.
- Klock HE, Koesema EJ, Knuth MW, Lesley SA. 2008. Combining the polymerase incomplete primer extension method for cloning and mutagenesis with microscreening to accelerate structural genomics efforts. *Proteins: Structure, Function, and Bioinformatics* 71: 982–994.
- Kumar S, Stecher G, Tamura K. 2016. MEGA7: molecular evolutionary genetics analysis v.7.0 for bigger datasets. *Molecular Biology and Evolution* 33: 1870–1874.
- Kurihara D, Mizuta Y, Sato Y, Higashiyama T. 2015. CLEARSEE: a rapid optical clearing reagent for whole-plant fluorescence imaging. *Development* 142: 4168–4179.
- Langmead B, Salzberg SL. 2012. Fast gapped-read alignment with BOWTIE 2. *Nature Methods* 9: 357–359.
- Lázaro A, Obeng-Hinne E, Albani MC. 2018. Extended vernalization regulates inflorescence fate in *Arabis alpina* by stably silencing PERPETUAL FLOWERING1. *Plant Physiology* 176: 2819–2883.
- Lázaro A, Zhou Y, Giesguth M, Nawaz K, Bergonzi S, Pecinka A, Coupland G, Albani MC. 2019. PERPETUAL FLOWERING2 coordinates the vernalization response and perennial flowering in *Arabis alpina*. *Journal of Experimental Botany* 70: 995–1004.
- Lee MH, Sano H. 2007. Attenuation of the hypersensitive response by an ATPase associated with various cellular activities (AAA) protein through suppression of a small GTPase, ADP ribosylation factor, in tobacco plants. *The Plant Journal* 51: 127–139.
- Letunic I, Bork P. 2019. Interactive Tree Of Life (ITOL) v.4: recent updates and new developments. *Nucleic Acids Research* 47: W256–W259.
- Li H, Handsaker B, Wysoker A, Fennell T, Ruan J, Homer N, Marth G, Abecasis G, Durbin R. 2009. The sequence alignment/map format and SAMtools. *Bioinformatics* 25: 2078–2079.
- Li P-C, Li K, Wang J, Zhao C-Z, Zhao S-Z, Hou L, Xia H, Ma C-L, Wang X-J. 2019a. The AAA-ATPase MIDASIN1 functions in ribosome biogenesis and is essential for embryo and root development. *Plant Physiology* 180: 289–304.
- Li P-C, Ma J-J, Zhou X-M, Li G-H, Zhao C-Z, Xia H, Fan S-J, Wang X-J. 2019b. *Arabidopsis* MDN1 is involved in the establishment of a normal seed proteome and seed germination. *Frontiers in Plant Science* 10: 1118.
- Li Z, Lathe RS, Li J, He H, Bhalerao RP. 2021. Towards understanding the biological foundations of perenniality. *Trends in Plant Science* 27: 56–58.
- Liu L, Li C, Teo ZWN, Zhang B, Yu H. 2019. The MCTP-SNARE complex regulates florigen transport in *Arabidopsis*. *Plant Cell* 31: 2475–2490.
- Liu X, Inoue H, Tang X, Tan Y, Xu X, Wang C, Jiang CJ. 2020. Rice OsAAA-ATPase1 is induced during blast infection in a salicylic acid-dependent manner, and promotes blast fungus resistance. *International Journal of Molecular Sciences* 21: 1443.
- Livak KJ, Schmittgen TD. 2001. Analysis of relative gene expression data using real-time quantitative PCR and the  $2^{-\Delta\Delta CT}$  method. *Methods* 25: 402–408.
- Micali CO, Neumann U, Grunewald D, Panstruga R, O’Connell R. 2011. Biogenesis of a specialized plant-fungal interface during host cell internalization of *Golovinomyces orontii* haustoria. *Cellular Microbiology* 13: 210–226.
- Moran DT, Rowley JC. 1987. Biological specimen preparation for correlative light and electron microscopy. In: Hayat MA, ed. *Correlative microscopy in biology*. Amsterdam, the Netherlands: Elsevier, 1–22.
- Mullen RT, Trelease RN. 2006. The ER-peroxisome connection in plants: development of the “ER semi-autonomous peroxisome maturation and replication” model for plant peroxisome biogenesis. *Biochimica et Biophysica Acta (BBA) – Molecular Cell Research* 1763: 1655–1668.
- Muralla R, Lloyd J, Meinke D. 2011. Molecular foundations of reproductive lethality in *Arabidopsis thaliana*. *PLoS ONE* 6: e28398.
- Musielak TJ, Slane D, Liebig C, Bayer M. 2016. A versatile optical clearing protocol for deep tissue imaging of fluorescent proteins in *Arabidopsis thaliana*. *PLoS ONE* 11: e0161107.
- Nix DA, Eisen MB. 2005. GATA: a graphic alignment tool for comparative sequence analysis. *BMC Bioinformatics* 6: 9.
- Ogura T, Wilkinson AJ. 2001. AAA + superfamily ATPases: common structure-diverse function. *Genes to Cells* 6: 575–597.
- Oikawa K, Hayashi M, Hayashi Y, Nishimura M. 2019. Re-evaluation of physical interaction between plant peroxisomes and other organelles using live-cell imaging techniques. *Journal of Integrative Plant Biology* 61: 836–852.
- Palmer WM, Martin AP, Flynn JR, Reed SL, White RG, Furbank RT, Grof CPL. 2015. PEA-CLARITY: 3D molecular imaging of whole plant organs. *Scientific Reports* 5: 13492.
- Park S, Rancour DM, Bednarek SY. 2008. *In planta* analysis of the cell cycle-dependent localization of AtCDC48A and its critical roles in cell division, expansion, and differentiation. *Plant Physiology* 148: 246–258.
- Reyes FC, Buono RA, Roschztardt H, Di Rubbo S, Yeun LH, Russinova E, Otegui MS. 2014. A novel endosomal sorting complex required for transport (ESCRT) component in *Arabidopsis thaliana* controls cell expansion and development. *Journal of Biological Chemistry* 289: 4980–4988.
- Riglet L, Rozier F, Kodera C, Bovio S, Sechet J, Fobis-Loisy I, Gaude T. 2020. KATANIN-dependent mechanical properties of the stigmatic cell wall mediate the pollen tube path in *Arabidopsis*. *eLife* 9: 1–21.
- Sawaguchi A, Ide S, Goto Y, Kawano J-I, Oinuma T, Suganuma T. 2001. A simple contrast enhancement by potassium permanganate oxidation for Lowicryl K4M ultrathin sections prepared by high pressure freezing/freezing substitution. *Journal of Microscopy* 201: 77–83.
- Schindelin J, Arganda-Carreras I, Frise E, Kaynig V, Longair M, Pietzsch T, Preibisch S, Rueden C, Saalfeld S, Schmid B *et al.* 2012. Fiji: an open-source platform for biological-image analysis. *Nature Methods* 9: 676–682.
- Schneeberger K, Ossowski S, Lanz C, Juul T, Petersen AH, Nielsen KL, Jørgensen J-E, Weigel D, Andersen SU. 2009. SHOREMAP: simultaneous mapping and mutation identification by deep sequencing. *Nature Methods* 6: 550–551.
- Schneider CA, Rasband WS, Eliceiri KW. 2012. NIH IMAGE to IMAGEJ: 25 years of image analysis. *Nature Methods* 9: 671–675.
- Shahriari M, Keshavaiah C, Scheuring D, Sabovljevic A, Pimpl P, Häusler RE, Hülskamp M, Schellmann S. 2010. The AAA-type ATPase AtSKD1 contributes to vacuolar maintenance of *Arabidopsis thaliana*. *The Plant Journal* 64: 71–85.
- Sheldon CC, Rouse DT, Finnegan EJ, Peacock WJ, Dennis ES. 2000. The molecular basis of vernalization: the central role of FLOWERING LOCUS C (FLO). *Proceedings of the National Academy of Sciences, USA* 97: 3753–3758.
- Sinclair AM, Trobacher CP, Mathur N, Greenwood JS, Mathur J. 2009. Peroxule extension over ER-defined paths constitutes a rapid subcellular response to hydroxyl stress. *The Plant Journal* 59: 231–242.
- Snider J, Thibault G, Houry WA. 2008. The AAA+ superfamily of functionally diverse proteins. *Genome Biology* 9: 216.
- Stemmer M, Thumberger T, del Sol KM, Wittbrodt J, Mateo JL. 2015. CCTOP: an intuitive, flexible and reliable CRISPR/Cas9 target prediction tool. *PLoS ONE* 10: e0124633.



- Stephan L, Tilmes V, Hülskamp M. 2019. Selection and validation of reference genes for quantitative Real-Time PCR in *Arabidopsis alpina*. *PLoS ONE* 14: e0211172.
- Sugimoto M, Yamaguchi Y, Nakamura K, Tatsumi Y, Sano H. 2004. A hypersensitive response-induced ATPase associated with various cellular activities (AAA) protein from tobacco plants. *Plant Molecular Biology* 56: 973–985.
- Sun H, Schneeberger K. 2015. SHOREMAP v.3.0: fast and accurate identification of causal mutations from forward genetic screens. In: Alonso JM, Stepanova AN, eds. *Methods in molecular biology*. New York, NY, USA: Humana Press, 381–395.
- Tang LP, Yang Y, Wang H, Li L, Liu L, Liu Y, Yuan J, Zhao XY, Palme K, Su YH *et al.* 2021. AtNSF regulates leaf serration by modulating intracellular trafficking of PIN1 in *Arabidopsis thaliana*. *Journal of Integrative Plant Biology* 63: 737–755.
- Ueda M, Matsui K, Ishiguro S, Sano R, Wada T, Paponov I, Palme K, Okada K. 2004. The HALTED ROOT gene encoding the 26S proteasome subunit RPT2a is essential for the maintenance of Arabidopsis meristems. *Development* 131: 2101–2111.
- Vayssières A, Mishra P, Roggen A, Neumann U, Ljung K, Albani MC. 2020. Vernalization shapes shoot architecture and ensures the maintenance of dormant buds in the perennial *Arabidopsis alpina*. *New Phytologist* 227: 99–115.
- Vukasić N, Žárský V. 2016. Tethering complexes in the Arabidopsis endomembrane system. *Frontiers in Cell and Developmental Biology* 4: 46.
- Wang R, Albani MC, Vincent C, Bergonzi S, Luan M, Bai Y, Kiefer C, Castillo R, Coupland G. 2011. AaTFL1 confers an age-dependent response to vernalization in perennial *Arabidopsis alpina*. *Plant Cell* 23: 1307–1321.
- Wang R, Farrona S, Vincent C, Joecker A, Schoof H, Turck F, Alonso-Blanco C, Coupland G, Albani MC. 2009. PEP1 regulates perennial flowering in *Arabidopsis alpina*. *Nature* 459: 423–427.
- Wang Z-P, Xing H-L, Dong L, Zhang H-Y, Han C-Y, Wang X-C, Chen Q-J. 2015. Egg cell-specific promoter-controlled CRISPR/Cas9 efficiently generates homozygous mutants for multiple target genes in Arabidopsis in a single generation. *Genome Biology* 16: 144.
- Wendler P, Ciniawsky S, Kock M, Kube S. 2012. Structure and function of the AAA+ nucleotide binding pocket. *Biochimica et Biophysica Acta – Molecular Cell Research* 1823: 2–14.
- White SR, Lauring B. 2007. AAA+ ATPases: achieving diversity of function with conserved machinery. *Traffic* 8: 1657–1667.
- Yedidi RS, Wendler P, Enekel C. 2017. AAA-ATPases in protein degradation. *Frontiers in Molecular Biosciences* 4: 42.
- Zhang B, Li C, Li Y, Yu H. 2020. Mobile TERMINAL FLOWER1 determines seed size in Arabidopsis. *Nature Plants* 6: 1146–1157.
- Zhang B, Van Aken O, Thatcher L, De Clercq I, Duncan O, Law SR, Murcha MW, van der Merwe M, Seifi HS, Carrie C *et al.* 2014. The mitochondrial outer membrane AAA ATPase AtOM66 affects cell death and pathogen resistance in *Arabidopsis thaliana*. *The Plant Journal* 80: 709–727.
- Zhang P, Zhang Y, Sun L, Sinumporn S, Yang Z, Sun B, Xuan D, Li Z, Yu P, Wu W *et al.* 2017. The rice AAA-ATPase OsFIGNL1 is essential for male meiosis. *Frontiers in Plant Science* 8: 1639.
- Zhou Y, Gan X, Viñeira de la Torre N, Neumann U, Albani MC. 2021. Beyond flowering time: diverse roles of an APETALA2-like transcription factor in shoot architecture and perennial traits. *New Phytologist* 229: 444–459.
- Zhu P, Lister C, Dean C. 2021. Cold-induced Arabidopsis FRIGIDA nuclear condensates for FLC repression. *Nature* 599: 657–661.
- Zhu X, Yin J, Liang S, Liang R, Zhou X, Chen Z, Zhao W, Wang J, Li W, He M *et al.* 2016. The Multivesicular Bodies (MVBs)-localized AAA ATPase LRD6-6 inhibits immunity and cell death likely through regulating MVBs-mediated vesicular trafficking in rice. *PLoS Genetics* 12: e1006311.
- Fig. S1** Causal mutations for *eop002*, *eop085* and *eop091* mutants are located on *Arabidopsis alpina* Chromosome 8.
- Fig. S2** The *Arabidopsis alpina eop002*, *eop085* and *eop091* mutants are allelic.
- Fig. S3** Fine-mapping of the causal mutation in the *Arabidopsis alpina* mutant *eop002*.
- Fig. S4** AaFRAT1 expression is reduced in *Arabidopsis alpina* dsRNAi transgenic lines.
- Fig. S5** The AaFRAT1 subclade shows an amino acid inversion of the core Walker B residues.
- Fig. S6** FRAT1 is expressed ubiquitously in *Arabidopsis thaliana* and *Arabidopsis alpina*.
- Fig. S7** Expression of *Arabidopsis alpina* floral promoters increases earlier in *eop002\_IL*.
- Fig. S8** AaFRAT1-VENUS complements the early-flowering phenotype of the *Arabidopsis alpina eop085* mutant.
- Fig. S9** AaFRAT1-VENUS accumulation patterns in *Arabidopsis alpina* do not change during development after cold exposure.
- Fig. S10** Transmission electron micrographs of longitudinal sections of *Arabidopsis alpina* primary roots after single immunogold labelling of AaFRAT1-VENUS.
- Fig. S11** Transmission electron micrographs of longitudinal serial sections of *Arabidopsis alpina* primary roots after single immunogold labelling of AaFRAT1-VENUS.
- Fig. S12** Mutations in AaFRAT1 or AtFRAT1 do not affect peroxisomal activity.
- Table S1** List of primers used in this study.
- Table S2** Single nucleotide polymorphisms detected by SHOREMAP in the *eop002* mutant.
- Table S3** Single nucleotide polymorphisms detected by SHOREMAP in the *eop085* mutant.
- Table S4** Single nucleotide polymorphisms detected by SHOREMAP in the *eop091* mutant.

## Supporting Information

Additional Supporting Information may be found online in the Supporting Information section at the end of the article.

Please note: Wiley Blackwell are not responsible for the content or functionality of any Supporting Information supplied by the authors. Any queries (other than missing material) should be directed to the *New Phytologist* Central Office.